International Conference on Nuclear Data for Science and Technology 2007
DOI: 10.1051/ndata:07496

The neutron capture cross sections of ^{237}Np(n,γ) and ^{240}Pu(n,γ) and its relevance in the transmutation of nuclear waste

C. Guerrero[1,a], U. Abbondanno[2], G. Aerts[3], H. Álvarez[4], F. Álvarez-Velarde[1], S. Andriamonje[3], J. Andrzejewski[5], P. Assimakopoulos[†6], L. Audouin[7], G. Badurek[8], P. Baumann[9], F. Bečvář[10], E. Berthoumieux[3], F. Calviño[11], M. Calviani[12,13], D. Cano-Ott[1], R. Capote[14,15], C. Carrapiço[3,16], P. Cennini[17], V. Chepel[18], E. Chiaveri[17], N. Colonna[19], G. Cortes[20], A. Couture[21], J. Cox[21], M. Dahlfors[17], S. David[7], I. Dillmann[22], C. Domingo-Pardo[22,23], W. Dridi[3], I. Duran[4], C. Eleftheriadis[24], M. Embid-Segura[1], L. Ferrant[†7], A. Ferrari[17], R. Ferreira-Marques[18], K. Fujii[2], W. Furman[25], I. Goncalves[18], E. González-Romero[1], F. Gramegna[12], F. Gunsing[3], B. Haas[26], R. Haight[27], M. Heil[22], A. Herrera-Martinez[17], M. Igashira[28], E. Jericha[8], F. Käppeler[22], Y. Kadi[17], D. Karadimos[6], D. Karamanis[6], M. Kerveno[9], P. Koehler[29], E. Kossionides[30], M. Krtička[10], C. Lampoudis[3,24], H. Leeb[8], A. Lindote[18], I. Lopes[18], M. Lozano[15], S. Lukic[9], J. Marganiec[5], S. Marrone[19], T. Martínez[1], C. Massimi[31], P. Mastinu[12], A. Mengoni[14,17], P.M. Milazzo[2], C. Moreau[2], M. Mosconi[22], F. Neves[18], H. Oberhummer[8], S. O'Brien[21], J. Pancin[3], C. Papachristodoulou[6], C. Papadopoulos[32], C. Paradela[4], N. Patronis[6], A. Pavlik[33], P. Pavlopoulos[34], L. Perrot[3], M.T. Pigni[8], R. Plag[22], A. Plompen[35], A. Plukis[3], A. Poch[20], J. Praena[12], C. Pretel[20], J. Quesada[15], T. Rauscher[36], R. Reifarth[27], C. Rubbia[37], G. Rudolf[9], P. Rullhusen[35], J. Salgado[16], C. Santos[16], L. Sarchiapone[17], I. Savvidis[24], C. Stephan[7], G. Tagliente[19], J.L. Tain[23], L. Tassan-Got[7], L. Tavora[16], R. Terlizzi[19], G. Vannini[31], P. Vaz[16], A. Ventura[38], D. Villamarin[1], M.C. Vincente[1], V. Vlachoudis[17], R. Vlastou[32], F. Voss[22], S. Walter[22], M. Wiescher[21], and K. Wisshak[22]

The n_TOF Collaboration (www.cern.ch/ntof)

[1]Centro de Investigaciones Energeticas Medioambientales y Tecnologicas, Madrid, Spain – [2]Istituto Nazionale di Fisica Nucleare, Trieste, Italy – [3]CEA/Saclay-DSM/DAPNIA, Gif-sur-Yvette, France – [4]Universidade de Santiago de Compostela, Spain – [5]University of Lodz, Lodz, Poland – [6]University of Ioannina, Greece – [7]Centre National de la Recherche Scientifique/IN2P3-IPN, Orsay, France – [8]Atominstitut der Österreichischen Universitäten, Technische Universität Wien, Austria – [9]Centre National de la Recherche Scientifique/IN2P3-IReS, Strasbourg, France – [10]Charles University, Prague, Czech Republic – [11]Universidad Politecnica de Madrid, Spain – [12]Istituto Nazionale di Fisica Nucleare, Laboratori Nazionali di Legnaro, Italy – [13]Dipartimento di Fisica, Università di Padova, Italy – [14]International Atomic Energy Agency (IAEA), Nuclear Data Section, Vienna, Austria – [15]Universidad de Sevilla, Spain – [16]Instituto Tecnológico e Nuclear (ITN), Lisbon, Portugal – [17]CERN, Geneva, Switzerland – [18]LIP - Coimbra & Departamento de Fisica da Universidade de Coimbra, Portugal – [19]Istituto Nazionale di Fisica Nucleare, Bari, Italy – [20]Universitat Politecnica de Catalunya, Barcelona, Spain – [21]University of Notre Dame, Notre Dame, USA – [22]Forschungszentrum Karlsruhe GmbH (FZK), Institut für Kernphysik, Germany – [23]Instituto de Física Corpuscular, CSIC-Universidad de Valencia, Spain – [24]Aristotle University of Thessaloniki, Greece – [25]Joint Institute for Nuclear Research, Frank Laboratory of Neutron Physics, Dubna, Russia – [26]Centre National de la Recherche Scientifique/IN2P3-CENBG, Bordeaux, France – [27]Los Alamos National Laboratory, New Mexico, USA – [28]Tokyo Institute of Technology, Tokyo, Japan – [29]Oak Ridge National Laboratory, Physics Division, Oak Ridge, USA – [30]NCSR, Athens, Greece – [31]Dipartimento di Fisica, Università di Bologna, and Sezione INFN di Bologna, Italy – [32]National Technical University of Athens, Greece – [33]Institut für Isotopenforschung und Kernphysik, Universität Wien, Austria – [34]Pôle Universitaire Léonard de Vinci, Paris-La Défense, France – [35]CEC-JRC-IRMM, Geel, Belgium – [36]Department of Physics-University of Basel, Switzerland – [37]Università degli Studi Pavia, Pavia, Italy – [38]ENEA, Bologna, Italy

Abstract. Neutron capture cross sections of actinides are of great relevance for the Transmutation of Nuclear Waste in Accelerator Driven Systems (ADS) and Generation-IV reactors. The neutron capture cross sections of ^{237}Np and ^{240}Pu were measured at the n_TOF facility with a Total Absorption Calorimeter. The data have been analyzed with the SAMMY code. The corresponding covariance matrices have been generated. The final cross sections are presented and compared to the previously existing ones.

1 Introduction

One of the solutions proposed for the management of radioactive nuclear waste is the transmutation. This technology could reduce substantially (by a factor of 1/100 or more) the radiotoxicity inventory of the long lived component of the nuclear waste, mainly the trans-uranium actinides. The detailed engineering designs, safety evaluations and the detailed performance assessment of dedicated transmutation ADS and critical reactors require more precise and complete basic nuclear data [1].

^{237}Np plays an important role because of two main reasons. First, it has the largest capture ratio after ^{239}Pu in a typical ADS core loaded with a fuel highly enriched in Minor Actinides (MA). Second, Np is the actinide element presenting the largest leakage probability from a deep underground repository. ^{240}Pu has also two main implications. First, ^{240}Pu is the second most abundant Pu isotope (after ^{239}Pu) in the

[a] Presenting author, e-mail: carlos.guerrero@ciemat.es

irradiated fuel discharged from a commercial Nuclear Power Plant. Second, ^{240}Pu can be the most abundant Pu isotope in the composition of the fuel for an ADS depending on the fuel cycle (open or closed).

The capture cross section of these two isotopes was measured at the n_TOF facility [2] during the 2004 campaign using the Total Absorption Calorimeter (TAC) in the energy range from 1 eV to 2 keV.

2 Measurement and experimental setup

The n_TOF facility and its performance in terms of neutron fluence, energy resolution, sources of background, etc., are described in detail in [2]. The targets of ^{237}Np (43.3 mg, 1.29 MBq) and ^{240}Pu (51.2 mg, 458 MBq) used in the measurements were sandwiched by two thin Al layers (total mass <75 mg) and canned inside a 0.35 mm thick Ti canning with ISO 2919 certification. Their isotopic purity was determined by γ-ray spectrometry and was better than 99% for ^{237}Np and about 90% for ^{240}Pu (with a 10% contamination of ^{239}Pu).

The neutron capture detection system consists of a segmented TAC made of 40 BaF_2 crystals with ^{10}B loaded carbon fiber capsules and placed at 185 m flight path from the spallation source. The TAC has nearly 100% detection efficiency for capture events and good energy resolution. The neutron sensitivity and the sample activity are reduced by using a $C_{12}H_{20}O_4(^6Li)_2$ neutron absorber placed between the sample and the cystals. The performance of the TAC has been investigated both experimentally, with calibration sources and the reference ^{197}Au(n,γ) cross section, and by Monte Carlo simulations [3,4].

The Data Acquisition system used in the measurements is fully based on digital electronics, with 54 channels of high performance 8 bits flash ADCs [5,6] (8 MBytes memory and 500 MSamples/s) recording the full detector history for neutron energy ranges between 0.3 eV and 20 GeV.

3 Procurement of the experimental capture yield

The experimental capture yield is defined as the fraction of neutrons entering the sample which undergo a capture reaction. It can be calculated as

$$Y(E_n) = \frac{C(E_{sum}, m_\gamma, E_n)}{\varepsilon_{DT}(E_n) N_{intercepted} \phi(E_n)} \quad (1)$$

where E_n is the neutron energy, E_{sum} and m_γ are deposited energy and crystal multiplicity respectively, $C(E_{sum}, m_\gamma, E_n)$ stands for the number of counts detected under the analysis conditions, $\varepsilon_{DT}(E_n)$ is the detection efficiency taking into account dead-time effects, $N_{intercepted}$ is the fraction of the beam intercepted by the sample ($radius_{sample}$ = 0.5 cm, $radius_{beam}$ ~2 cm) and $\phi(E_n)$ is the neutron fluence.

The best signal to background ratio in the data was found selecting events with $m_\gamma > 2$ and $2.5 < E_{sum}$ (MeV) < 6. Under these conditions, the detection efficiency of the TAC drops down to ~50% and shows a significant dependence on the particular nuclear electromagnetic (EM) de-excitation pattern and on the counting rate. The detection efficiency and its uncertainty (lower than 3%) have been calculated as a function of E_n for all the samples [7] by Monte Carlo simulation using the GEANT4 package [8].

All background components were characterized from the analysis of several dedicated measurements: background without neutron beam, Ti-canning without sample (capture and scattering in the Ti-canning), empty TAC with neutron beam (capture and scattering in any element but the Ti-canning and the sample) and ^{nat}C (neutron scattering at the sample).

The ^{237}Np elastic to capture cross section ratio is small and therefore the neutron sensitivity due to the ^{237}Np itself was found to be below 1% at all neutron energies. For the ^{240}Pu measurement there are isolated resonances for which the neutron sensitivity can be as high as 3%. In both cases the total background is characterized as a function of E_n and is taken into account in the cross section analysis.

4 Cross section analysis

The measured capture yields of ^{237}Np and ^{240}Pu have been analysed using the SAMMY code [9], following the iterative *SAMMY sequential fit method* in the resolved resonance region (RRR) [10,11]. The capture yields are analyzed together with transmission, using the resulting resonance parameters and covariance matrix of the fit to one data set as input for the next one. The results are a set of resonance parameters compatible with all data sets and a realistic covariance matrix. The transmission data are fitted first because of their a priori lower uncertainty in the normalization and background. If necessary, the various absolute normalizations are allowed to vary within their estimated uncertainties (5% for the n_TOF capture data) during the fits.

4.1 ^{237}Np cross section

In the RRR, below 500 eV, the ^{237}Np capture yield was analyzed together with the transmission data of Gressier et al. [12] measured at GELINA [13], included in the latest evaluations. The fits were performed in steps of 100 eV leaving the normalization, constant background and resonance parameters free for all resonances in the range under study. Figure 1 shows an example of the SAMMY fits to the three data sets.

Due to the small ^{237}Np level spacing, $D^{fitted}_{J=2-3}$ = 0.56 ± 0.02 eV, the resonances start to overlap above 140 eV. Therefore, the average radiative width is calculated only from resonances below 90 eV, resulting in $\langle \Gamma_\gamma^{RRR} \rangle = 41.5 \pm 0.8$ meV. This value was set as initial value for all resonances before the final sequential fit was performed, leaving $\Gamma_\gamma = \langle \Gamma_\gamma^{RRR} \rangle$ fixed for the small resonances. The neutron strength function S_0 was calculated as the variation with energy of the reduced neutron width $\Gamma_n^0 = \frac{\Gamma_n}{\sqrt{E}}$, resulting $S_0^{RRR} = (0.99 \pm 0.09) \times 10^{-4}$. The *unweighted average capture cross section* is calculated in steps of 50 eV and compared to the evaluated cross sections in figure 2. The n_TOF σ(n,γ) agrees with the evaluations below 300 eV, but it is lower by 5–10% at higher energies, which is also the case in the URR as discussed be low.

The n_TOF capture yield above 500 eV is transformed into capture cross section using the thin target approximation

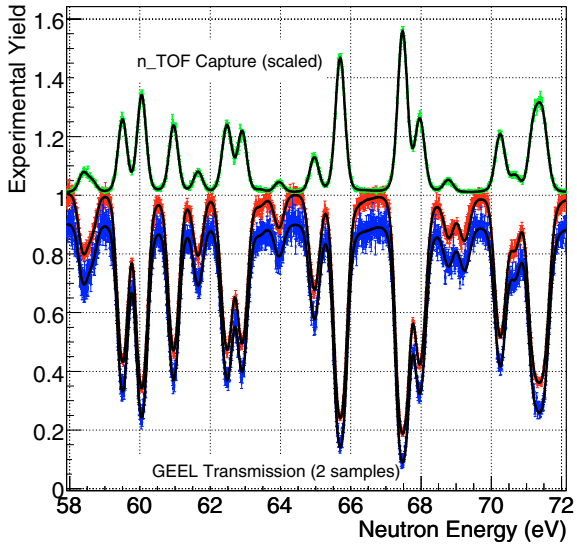

Fig. 1. SAMMY sequential fit to transmission (Gressier et al.) and capture (n_TOF). Colored-dots: experimental yield. Solid-lines: fitted yield.

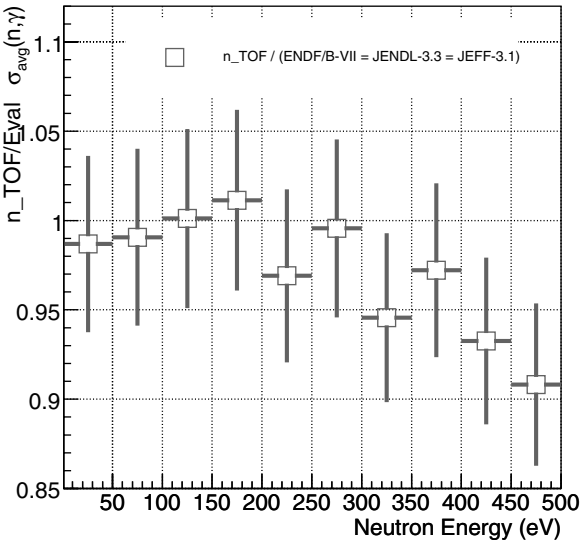

Fig. 2. n_TOF over evaluated ^{237}Np *unweighted average capture cross section* in the RRR.

(n_{at} = 1.401×10^4 at/barn). The code FITACS [14], included in SAMMY, was used to fit the average capture cross section with average resonance parameters from the Hauser-Feshbach calculation with width fluctuations. The values resulting from the fit are $\langle\Gamma_\gamma^{URR}\rangle$ = 40.1 ± 0.8 meV and S_0^{URR} = (0.97 ± 0.09) × 10^{-4}. These values agree within uncertainties with the results found in the RRR.

Figure 3 shows the n_TOF URR capture cross section compared to the evaluations files, all of them based on the measurements of Weston [15], and other experimental data. The ENDF/B-VII, JEFF-3.1 and JENDL-3.3 cross section are 10–15% above the n_TOF (as also happens in the 300–500 eV range of the RRR). Such a discrepancy in the cross section of the evaluated files is also observed in the values derived from the transmission measurement of Gressier (~10% uncertainty

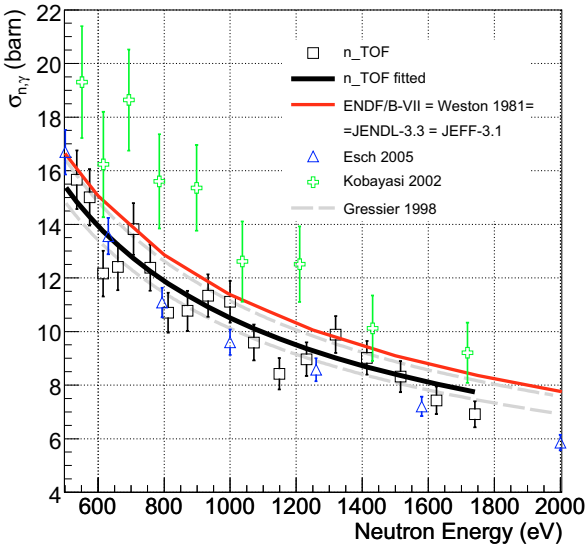

Fig. 3. ^{237}Np σ(n,γ) in the URR.

due to large correlations between $\langle\Gamma_\gamma^{URR}\rangle$ and S_0) and in the capture data from LANSCE (Esch et al.) [16]. However, the LANSCE data show a different dependence with energy from all other measurements. The capture data of Kobayashi, also shown in the figure, are systematicaly above all other measurements and evaluated data files.

4.2 ^{240}Pu cross section

The ^{240}Pu capture yield was analyzed following same procedure of the ^{237}Np resonance analysis. The n_TOF capture data are analyzed together with the transmission data of Kolar and Böckoff [17] (GELINA, 1968), also included in the work of Bouland et al. [10] and the evaluated data files. The ^{240}Pu level spacing is D ~ 12 eV and the resonances are well resolved up to several keV.

The ^{240}Pu sample used at n_TOF was inhomogeneous. This implies an uncertainty associated to the self-shielding that has been studied with the well known resonance at 1.056 eV. This uncertainty amounts to 20% from 1 to 10 eV, ~15–10% between 10 and 200 eV, ~5% up to 500 eV and negligible at higher energies. An accurate resonance analysis has been performed in the region between 500 eV and 2 keV.

The resulting values are $\langle\Gamma_\gamma^{RRR}\rangle$ = 32.4 ± 0.8 meV and S_0^{RRR} = 1.04 ± 0.05. Figure 4 shows the comparison between the n_TOF *unweighted average capture cross section* and different evaluated files. The n_TOF σ(n,γ) agrees with the JENDL-3.3 and JEFF-3.1 libraries except for some resonances around 800 eV, and is 5% to 20% larger than ENDF/B-VII.

5 Conclusions

The ^{237}Np and ^{240}Pu capture cross section have been measured at n_TOF in the range from 1 eV to 2 keV. The capture yield was calculated in reference to the ^{197}Au resonance at 4.9 eV. All instrumental effects such as the detection efficiency of the

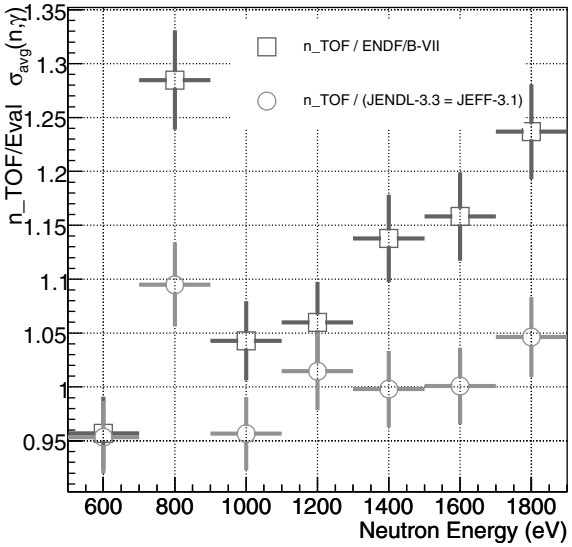

Fig. 4. n_TOF over evaluated ^{240}Pu *unweighted average capture cross section* in the RRR.

detector, dead-time losses, background, sample neutron sensitivity, etc. have been corrected yielding an overall uncertainty of 5%.

The capture yields have been analyzed using the SAMMY *sequential fit methodology*, including transmission measurements from GELINA, below 500 eV for the case ^{237}Np and below 2 keV for the ^{240}Pu. The FITACS code has been used for the analysis of the unresolved resonance region of ^{237}Np above 500 eV.

The n_TOF ^{237}Np σ(n,γ) is in agreement with the evaluated data files below ~300 eV and its is lower by 10 to 15% up to 2 keV. This discrepancy with the evaluated data files is also observed in the capture cross section derived from the transmission measurements of Gressier et al.

In the case of the ^{240}Pu σ(n,γ), the n_TOF σ(n,γ) agrees within uncertainties with JENDL-3.3 and JEFF-3.1, except for a group of resonances around 800 eV. ENDF/B-VII data are lower than n_TOF and the mentioned evaluations, with differences that increase with neutron energy up to 15–20%.

This work has been supported partially by the NTOF-ND-XADS project from the EU 5th Framework Programme, the CIEMAT-ENRESA Agreement on the "*separation and transmutation of nuclear waste*" and the Spanish Plan Nacional de Física de Partículas under contract FPA2005-06918-C03-01. The authors would like to thank G. Noguere from CEA-Cadarache for his help in the analysis of ^{237}Np transmission data.

References

1. G. Aliberti et al., Nucl. Sci. Eng. **146**, 13 (2004).
2. U. Abbondano et al., CERN/INTC-O-011, INTC-2002-037.
3. M. Heil et al., Nucl. Instrum. Meth. A **459**, 229 (2001).
4. D. Cano-Ott et al., *Proc. Int. Conf. on Capture Gamma-Ray Spectroscopy and Related Topics, CGS12, Notre Dame Indiana, USA, Sept. 4–9*, IP Conf. Proc. **819**, 318 (2005).
5. U. Abbondano et al., Nucl. Instrum. Meth. A **538**, 692 (2005).
6. http://www.acqiris.com/.
7. C. Guerrero et al. (The n_TOF Collaboration), *Workshop on Photon Strength Functions and Related Topics, Prague, Czech Republic, June 17–20* (2007).
8. S. Agostinelli et al., Nucl. Instrum Meth. A **506**, 250 (2003).
9. N.M. Larsson, ORNL/TM-9179/R7 (2006).
10. O. Bouland, H. Derrien, N.M. Larson, L.C. Leal, Nucl. Sci. Eng. **127**, 105 (1997).
11. H. Derrien, L.C. Leal, N.M. Larson, A. Courcelle, ORNL/TM-2005/241 (2005).
12. V. Gressier, DAPNIA/SPHN-99-04T.
13. http://www.irmm.jrc.be.
14. F.H. Fronher, B. Goel, U. Fischer, Report ANL-83-4 (1983).
15. L.W. Weston et al., Nuc. Sci. Eng. **79**, 184 (1981).
16. E.I. Esch, Los Alamos Scientific Lab. Reports **05**, 6885 (2005).
17. W. Kolar, K.H. Bockhoff, J. Nucl. Energy **22**, 299 (1968).